LANGMUIR

pubs.acs.org/Langmuir Article

Lipid Chemical Structure Modulates the Disruptive Effects of Nanomaterials on Membrane Models

Saeed Nazemidashtarjandi, Amid Vahedi, and Amir M. Farnoud*

Cite This: *Langmuir* 2020, 36, 4923–4932 Read Online

ACCESS | Metrics & More | Article Recommendations | Supporting Information

ABSTRACT: Understanding the mechanisms by which engineered nanomaterials disrupt the cell plasma membrane is crucial in advancing the industrial and biomedical applications of nanotechnology. While the role of nanoparticle properties in inducing membrane damage has received significant attention, the role of the lipid chemical structure in regulating such interactions is less explored. Here, we investigated the role of the lipid chemical structure in the disruption of lipid vesicles by unmodified silica, carboxyl-modified silica, and unmodified polystyrene nanoparticles (50 nm). The role of the lipid headgroup was examined by comparing nanoparticle effects on vesicles composed of 1,2-dioleoyl-*sn*-glycero-3-phosphocholine (DOPC) vs an inverse phosphocholine (PC) with the same acyl chain structure. The role of acyl chain saturation was examined by comparing nanoparticle effects on saturated vs unsaturated PCs and sphingomyelins. Nanoparticle effects on PCs (glycerol backbone) vs sphingomyelins (sphingosine backbone) were also examined. Results showed that the lipid headgroup, backbone, and acyl chain saturation affect nanoparticle binding to and disruption of the membranes. A low headgroup tilt angle and the presence of a trimethylammonium moiety at the vesicle surface are required for unmodified nanoparticles to induce membrane disruption. Lipid backbone structure significantly affects nanoparticle−membrane interactions, with carboxyl-modified particles only disrupting lipids containing cis unsaturation and a sphingosine backbone. Acyl chain saturation makes vesicles more resistant to particles by increasing lipid packing in vesicles, impeding molecular interactions. Finally, nanoparticles were capable of changing the lipid packing, resulting in pore formation in the process. These observations are important in interpreting nanoparticle toxicity to biological membranes.

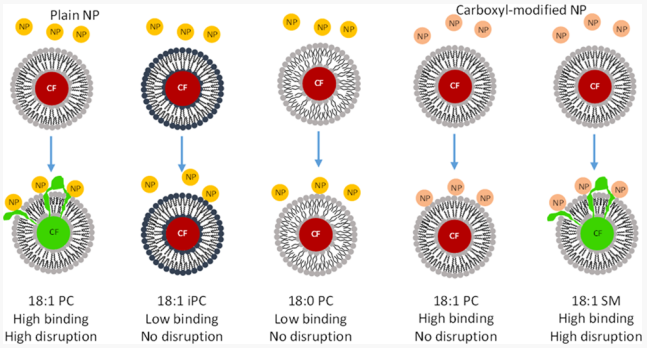

INTRODUCTION

The 21st century has seen unprecedented incorporation of nanomaterials in consumer products.[1,2] In addition, there has been a rise in the use of nanomaterials in biomedical research as carriers for the delivery of genes, drugs, and imaging agents.[3,4] This widespread use of nanomaterials in industrial and biomedical applications has raised concerns about their potential adverse effects on mammalian cells. The cell plasma membrane, a lipid bilayer that separates that cell from the extracellular environment, is the first cellular entity that comes into direct contact with exogenous particles. Interactions of nanomaterials with the plasma membrane have been demonstrated to alter membrane properties such as lipid packing,[5,6] membrane potential,[7,8] membrane permeability,[9,10] and membrane integrity,[11] thereby affecting normal cell functions. A detailed understanding of how nanoparticle and plasma membrane properties each contribute to nanoparticle-induced alterations in membrane properties is necessary to better understand the mechanisms by which nanoparticles induce cellular toxicity.

Due to the complex and dynamic structure of the cell plasma membrane, phospholipid bilayers, primarily lipid vesicles, are commonly exploited as models to facilitate mechanistic studies of nanoparticle−membrane interactions.[12] Previous studies have provided a valuable insight into the role of nanoparticle properties, such as size,[13,14] surface charge,[15−17] shape,[18] and surface chemistry,[19,20] in affecting membrane integrity. However, such studies have been primarily focused on the properties of engineered nanomaterials, and there has been little investigation into the role of the lipid chemical structure, including headgroup, backbone, and acyl chain saturation, and the resulting differences in lipid packing, in regulating nanoparticle-induced membrane damage. Understanding the role of lipid chemical structure in nanoparticle-induced membrane damage can aid in predicting the toxicity of nanomaterials to cells depending on their membrane lipid

Received: February 1, 2020
Revised: April 20, 2020
Published: April 21, 2020

https://dx.doi.org/10.1021/acs.langmuir.0c00295
Langmuir 2020, 36, 4923−4932

composition. Providing such information is important as different cells have different membrane lipid compositions and could therefore show differences in their interactions with nanomaterials.[21,22]

In a previous study, we showed that engineered silica nanoparticles (50 nm) interact differently with vesicles mimicking the lipid composition of the outer or the inner leaflet of the plasma membrane of red blood cells, suggesting a clear role for membrane lipid composition in regulating nanoparticle−membrane interactions.[23] In addition, we found that unmodified and carboxyl-modified silica nanoparticles with similar size and charge show differences in their disruptive effects on lipid membranes.[23] While electrostatic forces between nanoparticles and membrane lipids are commonly proposed as the primary mechanism through which nanoparticles bind to and induce damage in lipid membranes, our findings suggested that nanoparticle−lipid interactions, even for nanoparticles of similar charge, depend on both the chemical moieties on nanoparticle surfaces and the chemical structure of the lipids in the membrane.

In the current study, we examined the role of the lipid chemical structure and nanoparticle surface moieties in regulating nanoparticle−membrane interactions in more detail. Single-component phospholipid vesicles with different headgroup, backbone, and acyl chain structures were used to prevent phase separation and subsequent redistribution of vesicle components, thereby providing simple vesicle models to study the role of lipid chemical structure in regulating the disruptive effects of nanomaterials. Studies focused on phosphatidylcholine (PC) and sphingomyelin (SM) species, which are two predominant phospholipids in the outer leaflet of the cell plasma membrane of eukaryotes.[24−26] Unmodified (plain) and carboxyl-modified silica as well as unmodified polystyrene (all with a nominal diameter of 50 nm) were used as particle models. Silica nanoparticles have been used in consumer products such as cosmetics,[27−29] paint,[30] and textile industry[31] and also employed in biomedical research as drug and gene carriers.[27−29] Polystyrene nanoparticles have also been widely used as a model particle in biomedical research[32,33] and allow for understanding of the role of the particle core composition. Our studies show that, while nanoparticle properties are important in the outcome of nanoparticle−membrane interactions, so is the lipid chemical structure, and slight changes in lipid molecules result in significant differences in nanoparticle-induced membrane damage.

EXPERIMENTAL SECTION

Materials. Lipids including 1,2-dioleoyl-*sn*-glycero-3-phosphocholine (18:1 PC, DOPC), 2-((2,3-bis(oleoyloxy)propyl)-dimethylammonio)ethyl hydrogen phosphate (18:1 iPC, DOCP), 1,2-distearoyl-*sn*-glycero-3-phosphocholine (18:0 PC, DSPC), *N*-stearoyl-D-erythro-sphingosylphosphorylcholine (18:0 SM (d18:1/18:0)), *N*-oleoyl-D-erythro-sphingosylphosphorylcholine (18:1 SM (d18:1/18:1(9Z))), 1,2-dioleoyl-*sn*-glycero-3-phosphoethanolamine-*N*-(lissamine rhodamine B sulfonyl) (18:1 Liss Rhod-PE), and 1,2-dipalmitoyl-*sn*-glycero-3-phosphoethanolamine-*N*-(lissamine rhodamine B sulfonyl) (ammonium salt) (16:0 Liss Rhod-PE) were purchased from Avanti Polar Lipids (Alabaster, AL). Triton X-100, 5(6)-carboxyfluorescein (CF), and 1,6-diphenyl-1,3,5-hexatriene (DPH) were obtained from Sigma-Aldrich (St. Louis, MO). Phosphate-buffered saline (PBS, 10×) powder was obtained from Fisher BioReagents (Fair Lawn, NJ). Fluorescent silica nanoparticles (50 nm), either unmodified or carboxyl-modified, and fluorescent unmodified polystyrene nanoparticles (50 nm) with sulfonic chemical group (−SO3H) were purchased from Micromod Partkeltechnologie GMBH (Rostock, Germany).

Preparation of Multilamellar and Unilamellar Vesicles. Large unilamellar vesicles (LUVs) of 18:1 PC, 18:1 iPC, 18:0 PC, 18:0 SM, and 18:1 SM were prepared as previously described.[20,23] Briefly, individual lipids, dissolved in chloroform, were dried using a SpeedVac (Thermo Fisher, Waltham, MA). Lipid films were hydrated with PBS at 70 °C and vortex-mixed for 15 min to prepare multilamellar vesicles (MLVs). Subsequently, LUVs were prepared by subjecting the MLVs to 7 cycles of freezing in an acetone bath placed in dried ice for 3 min and thawing in water bath at 70 °C for 3 min. The prepared mixtures were then passed through a polycarbonate filter with a pore size of 100 nm (Avanti Polar Lipids) 11 times at 60 °C to obtain uniform symmetric vesicles. To prepare CF-encapsulated LUVs, the aforementioned protocol was used except that lipids were hydrated with a CF solution (∼80 mM) containing 30 mg of CF dissolved in 790 μL of PBS and 210 μL of 1M NaOH (final PH = 7.3), instead of PBS. The prepared vesicles were then passed through disposable PD-10 desalting columns containing a Sephadex G-25 medium to separate the excess, nonencapsulated CF. CF-encapsulated LUVs were used directly for vesicle leakage experiments.

Vesicle Leakage. To examine the effects of nanoparticles on vesicle integrity, vesicle leakage assays were performed. For these experiments, CF-encapsulated vesicles were used. Leakage of CF from the vesicles was measured using a Synergy H1 microplate reader spectrophotometer (Biotek, Winooski, VT). Prepared CF-encapsulated LUVs (5 mM) were diluted to a concentration of 50 μM in a black flat-bottom 96-well plate for the leakage experiments. The samples were excited at a wavelength of 492 nm and monitored for their fluorescence intensity at an emission wavelength of 517 nm, every 150 s over the course of 60 min at 25 °C. Triton X-100 with a concentration of 0.2% (v/v) was used to disrupt vesicles completely and release the encapsulated CF. The fluorescence intensity obtained from detergent-treated vesicles was considered as 100% leakage. CF leakage percentage was calculated using the following equation

$$\%\text{Leakage} = (F_T - F_0)/(F_{100} - F_0) \quad (1)$$

where F_T is the fluorescence intensity measured at each interval, F_0 is the fluorescence intensity of the control before adding particles, and F_{100} is the fluorescence intensity of the vesicles that were completely disrupted by a detergent. Leakage experiments with the particles were performed similarly after adding the particles to the 96-well plate that contained vesicles. Experiments were performed at particle concentrations of 0.0001, 0.001, and 0.01 g/L, corresponding to 1.34, 13.4, and 134 pM for silica nanoparticles and 2.46, 24.6, and 246 pM for polystyrene nanoparticles. All experiments were conducted for a minimum of three independent replicates.

Förster Resonance Energy-Transfer (FRET) Experiments. Förster resonance energy transfer (FRET) was performed to examine particle association with vesicles. To ensure homogeneous lipid distribution in vesicles, 18:1 rhodamine-PE (18:1 Rhod-PE) and 16:0 rhodamine-PE (16:0 Rhod-PE) were incorporated into the vesicles during synthesis, depending on the lipid acyl chain structure. For the lipid vesicles with unsaturated acyl chains, including 18:1 PC, 18:1 iPC, and 18:1 SM, 18:1 Rhod-PE was used, while for lipids containing saturated acyl chains, 16:0 Rhod-PE was utilized. LUVs were suspended inside 96-well plates. Fluorescent nanoparticles, the surface of which was functionalized with fluorescein (FRET donor), were then added to the vesicle suspension (F samples). F_0 samples had a mixture of pure vesicles, without the Rhod-PE (FRET acceptor), but with fluorescent nanoparticles. The background for F samples contained vesicles with the same amount of acceptor in the F samples without particles. Background for F_0 samples contained pure vesicles without Rhod-PE. For FRET experiments, vesicles were prepared at the same concentration used for the leakage experiments and were incubated with particles for 1 h at 25 °C. The F and F_0 fluorescence intensities were measured and the ratio of F/F_0 was calculated for each sample after 1 h. All experiments were performed at least 3 independent times to estimate uncertainties.

https://dx.doi.org/10.1021/acs.langmuir.0c00295
Langmuir 2020, 36, 4923−4932

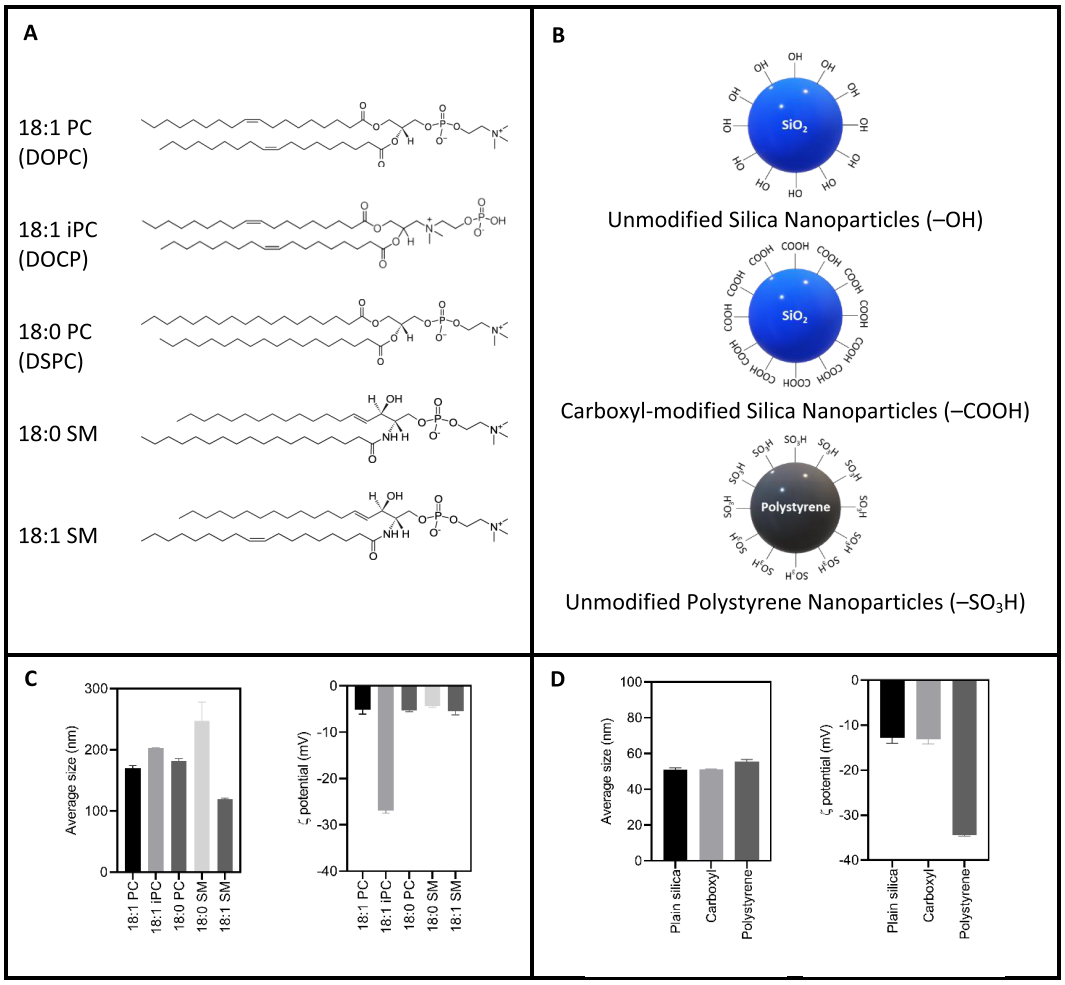

Figure 1. Nanoparticle and vesicle characterization. (A) Chemical structure of lipids and (B) schematic of nanoparticles used in this study. (C) Average size (diameter) and ζ-potential of single-component vesicles at PH = 7.4 in PBS. (D) Average size (diameter) and ζ-potential of nanoparticles at PH = 7.4 in PBS.

DPH Anisotropy. Fluorescence anisotropy was carried out using a Fluorolog-3 spectrofluorometer (Horiba Scientific, Edison, NJ). DPH anisotropy was used to assess lipid packing in vesicles before and after interaction with nanoparticles. Anisotropy is the ratio of the subtraction of polarized components of the emitted light intensity to the total fluorescence intensity of DPH emission. The lipophilic fluorescent probe DPH was dissolved in acetone and added to pre-prepared LUV suspension at a concentration of 0.2 mol %. Vesicle concentration at which DPH anisotropy was performed was similar to the vesicle leakage, as well as the FRET assay experiments (50 μM). Anisotropy measurements were carried out at 25 °C. For samples with no particles, DPH was added to the samples and anisotropy was measured after 1 h of incubation. To measure the anisotropy of vesicles after interaction with particles, vesicles were first exposed to particles at concentrations of 0.01 and 0.1 mg/mL (corresponding to 134 and 1340 pM for silica and 246 and 2460 pM for polystyrene nanoparticles) for 1 h. DPH was then added to the vesicles and anisotropy was measured.

Size and ζ-Potential Measurement. The size distribution and ζ-potential of nanoparticles and lipid vesicles were measured using a Zetasizer Nano ZS (Malvern Instruments Ltd., Worcestershire, U.K.). Particle suspensions were prepared in PBS at a concentration of 0.01 mg/mL (134 pM for silica and 246 pM for polystyrene nanoparticles). In addition, the size and ζ-potential of lipid vesicles were measured in PBS at the same concentration used for all other assays (50 μM).

Statistical Analysis. All experiments in this study were performed a minimum of three independent replicates. All statistical analysis was performed using the Graphpad Prism software package (La Jolla, CA). The average and standard deviation (mean ± standard deviation) were reported for all experiments. *P*-values were used as a criterion for significance with a *p*-value of <0.05 considered statistically significant. The following symbols were used to denote significance in all figures: $*P < 0.05$, $**P < 0.01$, $***P < 0.001$. *P*-values of >0.05 were shown as n.s. (not significant). One-way or two-way analysis of variance (ANOVA) with Dunnett's, Tukey's, or Sidak's post hoc was used depending on the statistical comparison that was needed.

RESULTS AND DISCUSSION

Lipid and Nanoparticle Models. SMs and PCs were used as model lipids in this study. PCs, terminated by phosphate and choline, with unsaturated, 1,2-dioleoyl-*sn*-glycero-3-phosphocholine (18:1 (9*Z*) PC, DOPC), or saturated, 1,2-distearoyl-*sn*-glycero-3-phosphocholine (18:0 PC, DSPC), acyl chains were used to examine the role of chain saturation in nanoparticle–lipid interactions. In addition, 2-((2,3-bis(oleoyloxy)propyl) dimethylammonio) ethyl hydrogen phosphate (18:1 (9*Z*) inverse PC (iPC), DOCP) was also used. This synthetic lipid contains an inverted headgroup, in which the phosphate moiety is exposed to the surface instead of the trimethylammonium group in normal PCs. It should also be noted that iPC is a synthetic lipid that, to the best of our knowledge, does not exist in eukaryotes or prokaryotes and was only used to elucidate the role of the moieties exposed at

https://dx.doi.org/10.1021/acs.langmuir.0c00295
Langmuir 2020, 36, 4923−4932

the surface of lipids in their interaction with nanoparticles. Two SMs were also used in this study. While SMs are also classified as phospholipids, they contain a sphingosine backbone, which distinguishes them from PCs, which have a glycerol backbone. *N*-Stearoyl-D-erythro-sphingosylphosphorylcholine (18:0 SM, d18:1/18:0) and *N*-oleoyl-D-erythro-sphingosylphosphorylcholine (18:1 SM, d18:1/18:1(9*Z*)) were employed as SM models. These lipids differ in their saturation levels, which allows for studies on the role of acyl chain saturation in SMs, as well as PCs. The chemical structure of all of the lipids used in this study is shown in Figure 1A.

Silica and polystyrene nanoparticles, with a nominal diameter of 50 nm, were used as nanoparticle models. The use of unmodified and carboxyl-modified silica, which have similar charge and size properties, allowed for comparison of the role of the surface moiety (i.e., silanol vs carboxyl) in nanoparticle−membrane interactions. It should be noted that some silanol moieties still exist on the surface of carboxyl-modified silica nanoparticles since the carboxyl chemical group is covalently attached to the surface of the unmodified silica nanoparticles, which contain silanol on their surface. To eliminate the possible effects of silanol on the surface of carboxyl-modified silica, and also to study the effect of a different core composition, unmodified polystyrene nanoparticles were also used. It should be noted that, although the polystyrene particles are not coated with other chemical moieties, and are referred to as unmodified particles throughout, sulfonic chemical groups used in the process of particle synthesis appear on the surface of these particles.[34] A schematic of the nanoparticles used in this study and their surface chemical groups is shown in Figure 1B.

Vesicle and Nanoparticle Characterization. Large unilamellar vesicles (LUVs) were synthesized and characterized by measuring their average size, hydrodynamic diameter, and ζ-potential using dynamic light scattering (Figure 1C). For all compositions, the vesicle diameter ranged between 100 and 250 nm, with some size deviations observed as a function of lipid composition. The ζ-potential of the PC and SM vesicles was in the narrow range of −4.0 to −6.0 mV (Figure 1C); however, the ζ-potential of iPC was highly negative (−26.9 ± 0.6 mV) due to the presence of phosphate at the extremity of this molecule. It should also be noted that vesicles containing 18:1 PC, 18:1 iPC, and 18:1 SM are in the liquid-disordered (L_d) phase, while 18:0 PC and 18:0 SM vesicles are in the liquid-ordered (L_o) phase, due to the saturation of their acyl chains, which results in high melting temperatures.[35,36]

In addition to vesicle characterization, the size and ζ-potential of nanoparticles were measured in phosphate-buffered saline (PBS). For all nanoparticles, the average size was in the range of 50 nm (Figure 1D). The size distribution of nanoparticles was also examined after 1 h of incubation in PBS, the same medium used for studies of nanoparticle−vesicle interaction, and no significant aggregation of particles was observed (Figure S1). The ζ-potential of unmodified and carboxyl-modified silica nanoparticles was −12.8 ± 1.2 and −13.1 ± 1.1 mV, respectively, showing no significant difference in their surface charge (Figure 1D). However, the ζ-potential of polystyrene nanoparticles was significantly greater than that of silica nanoparticles (−34.4 ± 0.3 mV) due to the lower pK_a of sulfonic chemical moiety that presents on the surface of polystyrene (Figure 1D).

Nanoparticle-Induced Membrane Damage Depends on Both Nanoparticle Surface Chemistry and Lipid Chemical Structure. Nanoparticle effects on the integrity of the different vesicles were investigated using the well-known vesicle leakage assay.[20,23] To perform this assay, 5(6)-carboxyfluorescein (CF) was encapsulated in vesicles at a high concentration (>80 mM), resulting in self-quenching of the dye. An alteration in the integrity of the vesicles that leads to the release of CF to the medium results in dilution of CF and higher fluorescence intensity, which can be used to monitor vesicle integrity. The interactions of vesicles with unmodified silica and polystyrene, as well as carboxyl-modified silica nanoparticles, were then investigated. Vesicles, at a concentration of 50 μM, were exposed to silica nanoparticles at particle concentrations of 1.34, 13.4, and 134 pM and to polystyrene nanoparticles at concentrations of 2.46, 24.6, and 246 pM. Note that these molar concentrations correspond to mass concentrations of 0.0001, 0.001, and 0.01 mg/mL for all particles. The extent of CF leakage from the lumen of vesicles after exposure to nanoparticles was evaluated and used as a measure of the loss of vesicle integrity. Vesicles in PBS, without nanoparticles, and vesicles exposed to Triton X-100 were used as negative and positive control, respectively.

Nanoparticle effects on vesicle integrity showed a significant dependence on lipid chemical structure. Unmodified silica nanoparticles (134 pM) induced a significant disruption in 18:1 PC vesicles, as evidenced by high CF leakage (Figure 2A). Nanoparticle-induced vesicle disruption was reduced significantly in 18:1 iPC vesicles, which contain an inverted headgroup. Since 18:1 PC and 18:1 iPC vesicles contain identical acyl unsaturation and tail length, these results indicate that the chemical group exposed at the vesicle surface plays an important in nanoparticle-induced vesicle damage. In contrast to 18:1 PC and 18:1 SM vesicles, unmodified silica nanoparticles did not induce appreciable disruption in 18:0 PC and 18:0 SM vesicles, suggesting that acyl chain saturation, resulting in highly ordered lipids, enhances the resistance of vesicles to the disruptive effects of nanoparticles (Figure 2A). While the extent of dye leakage induced by unmodified polystyrene nanoparticles was different compared to that induced by unmodified silica, both nanoparticles showed disruptive effects on the same set of vesicles. Polystyrene particles disrupted 18:1 PC and 18:1 SM vesicles, while the level of disruption was reduced in 18:1 iPC and abrogated in 18:0 PC and 18:0 SM (Figure 2B). Taken together, results indicate that nanoparticles are more disruptive to those vesicles in which choline is exposed at the surface and are in the L_d phase.

Studies with carboxyl-modified silica elucidated that in addition to the lipid chemical structure, the surface properties of nanoparticles highly affect vesicle integrity. In stark contrast to the observations with unmodified silica and polystyrene, carboxyl-modified silica showed little to no disruption on any of the vesicles except for 18:1 SM (Figure 2C). The observation that carboxyl-modified silica particles disrupted 18:1 SM vesicles, but not 18:1 PC vesicles, which contain the same cis unsaturation but a glycerol backbone, suggests that the carboxylic group has strong interaction with sphingosine backbone in 18:1 SM vesicle. A question may be raised regarding the lack of disruption of 18:0 SM vesicles, which also contains a sphingosine backbone, by carboxyl-modified silica. This stems from the fact that 18:0 SM vesicles are in a highly ordered (L_o) state due to the saturation of the acyl chain; therefore, the sphingosine backbone is less accessible to the carboxyl chemical moiety on the nanoparticles. It should be

https://dx.doi.org/10.1021/acs.langmuir.0c00295
Langmuir 2020, 36, 4923−4932

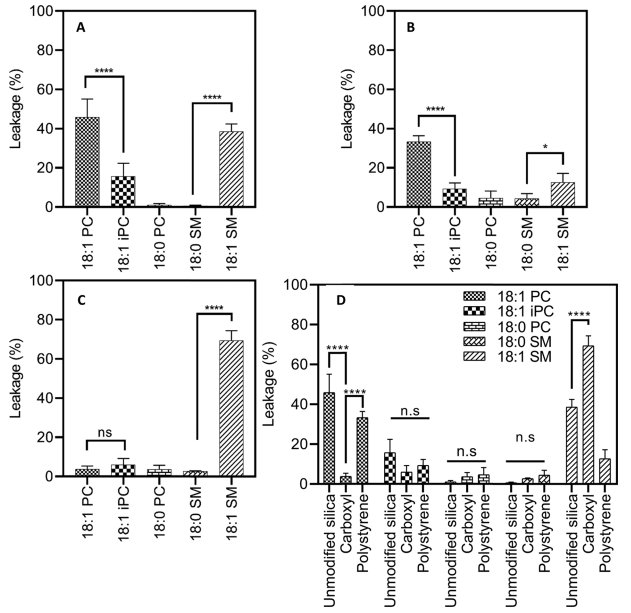

Figure 2. Leakage of CF from single-component vesicles induced by nanoparticles at a concentration of 134 pM (0.01 mg/mL) for silica and 246 pM (0.01 mg/mL) for unmodified polystyrene following incubation at 25 °C in PBS for 1 h for (A) 50 nm unmodified silica nanoparticles, (B) 50 nm unmodified polystyrene nanoparticles, and (C) 50 nm carboxyl-modified silica nanoparticles. (D) Side-by-side comparison of percent leakage induced by all of the nanoparticles in each vesicle after 1 h. Error bars demonstrate the standard deviation from at least three independent experiments. (A) One-way ANOVA with Tukey's post hoc test, at 1 h post-incubation comparing the leakage of vesicles induced by 50 nm unmodified silica particles: ****P(18:1 PC vs 18:1 iPC) <0.0001, ****P(18:0 SM vs 18:1 SM) <0.0001; (B) one-way ANOVA with Tukey's post hoc test, at 1 h post-incubation comparing the leakage of vesicles induced by 50 nm unmodified polystyrene particles: ****P(18:1 PC vs 18:1 iPC) <0.0001, *P(18:0 SM vs 18:1 SM) <0.03; (C) one-way ANOVA with Tukey's post hoc test, at 1 h post-incubation comparing the leakage of vesicles induced by 50 nm carboxyl-modified silica particles: comparing the leakage of 18:1 PC vesicle with 18:1 iPC vesicle did not show any significant difference, ****P(18:0 SM vs 18:1 SM) <0.0001; and (D) following p-values were obtained using two-way ANOVA with Sidak's post hoc test comparing vesicle leakage induced by unmodified silica, carboxyl-modified silica, and polystyrene particles: for 18:1 PC vesicle: ****P(silica vs carboxyl) <0.0001, ****P(carboxyl vs polystyrene) <0.0001, for 18:1 iPC vesicle: no significant difference in vesicle leakage induced by nanoparticles was observed, for 18:0 PC: no significant difference in vesicle leakage induced by nanoparticles was observed, for 18:0 SM: no significant difference in vesicle leakage induced by nanoparticles was observed, for 18:1 SM: ****P(silica vs carboxyl) <0.0001.

noted that the disruptive effects of nanoparticles on all vesicles were dose-dependent. In most cases, a time-dependent leakage was also observed with the leakage starting immediately after vesicle exposure to nanoparticles and reaching equilibrium after approximately 15 min (Figures S2−S4).

The importance of nanoparticle properties, as well as the lipid chemical structure in regulating nanoparticle-induced membrane damage, is elucidated by the side-by-side comparison of the disruptive effects of nanoparticles on different membranes. Comparing the extent of leakage in vesicles induced by nanoparticles (Figure 2D) suggests that nanoparticles containing different surface moieties induced similar dye leakage in 18:1 iPC, 18:0 PC, and 18:0 SM vesicles. However, significant differences in nanoparticle-induced disruption were observed in 18:1 SM and 18:1 PC vesicles. Since nanoparticles have a negative ζ-potential and similar size, these results suggest that the specific chemical moieties on the particle surface and in the lipid structure, and not just pure electrostatics, determine whether nanoparticles induce damage in the membrane.

Nanoparticles Bind to Highly Fluid Vesicles That Contain Choline at the Surface. Nanoparticle localization on vesicle surfaces is a preliminary step in the induction of membrane disruption.[37] To examine nanoparticle binding to vesicles, a Förster resonance energy-transfer (FRET)-based assay, developed earlier by our group,[23] was utilized. In this assay, fluorescein on nanoparticles (E_x: 485 nm, E_m: 515 nm) and Rhod-PE (1 mol %, E_x: 560 nm, E_m: 583 nm) incorporated into the vesicles were used as FRET donor and acceptor, respectively. FRET only occurs if the FRET pair is in close proximity, in the nano-scale range,[36] allowing us to study nanoparticle localization on vesicle surfaces, by monitoring the quenching of fluorescein on nanoparticles by rhodamine on the vesicle surfaces. F/F_0, which is the ratio of the fluorescence intensity of the donor in the presence of the acceptor to the intensity of the donor in the absence of the acceptor, was then calculated. F/F_0 takes a value between 0 and 1. Low values of F/F_0 indicate a high level of FRET efficiency. Thus, a low F/F_0 is expected when a significant amount of nanoparticles are in close proximity to the vesicles. In contrast, a high F/F_0 is expected when there is a lack of significant binding. Note that the FRET signal in this assay might not only result from nanoparticle binding to vesicles but also result from vesicle wrapping around the particles and even bilayer formation on particle surfaces. Thus, the FRET signal comes from the nanoparticle−vesicle association of any kind (binding, wrapping, bilayer formation), which results in fluorescence quenching due to the particles being in close proximity to the vesicles. Vesicles composed of saturated lipids are expected to be primarily in the L_o phase, and vesicles composed of unsaturated lipids are expected to be in the L_d phase. Therefore, 16:0 Rhod-PE was used in the L_o phase vesicles, while 18:1 Rhod-PE was used in the L_d phase vesicles to ensure a homogeneous distribution of the dye.

Using the FRET-based assay, nanoparticles were observed to associate with vesicles in the L_d phase to a greater extent compared to those in the L_o phase. Unmodified silica nanoparticles, at a concentration of 134 pM, associated to a great extent with 18:1 PC and 18:1 SM vesicles, as evidenced by low F/F_0, but their binding to 18:1 iPC vesicles was reduced significantly, as evidenced by high F/F_0 (Figure 3A). Background fluorescence intensity for the samples, as well as raw FRET data, can be found in Tables S1−S3. Unmodified silica nanoparticles did not associate with vesicles in the L_o phase, including 18:0 PC and 18:0 SM vesicles, to a significant extent (high F/F_0), demonstrating that acyl chain saturation affects nanoparticle−vesicle association (Figure 3A). Similar results were observed for unmodified polystyrene and carboxyl-modified silica nanoparticles (Figure 3B,C). These particles significantly associated with 18:1 PC and 18:1 SM vesicles, but the extent of nanoparticle−vesicle association was decreased in 18:1 iPC. In addition, polystyrene and carboxyl-modified silica did not associate with 18:0 PC and 18:0 SM vesicles to a significant degree. Comparing the extent of nanoparticle binding with all vesicles revealed that nanoparticles with different surface properties associated to a similar extent with

https://dx.doi.org/10.1021/acs.langmuir.0c00295
Langmuir 2020, 36, 4923−4932

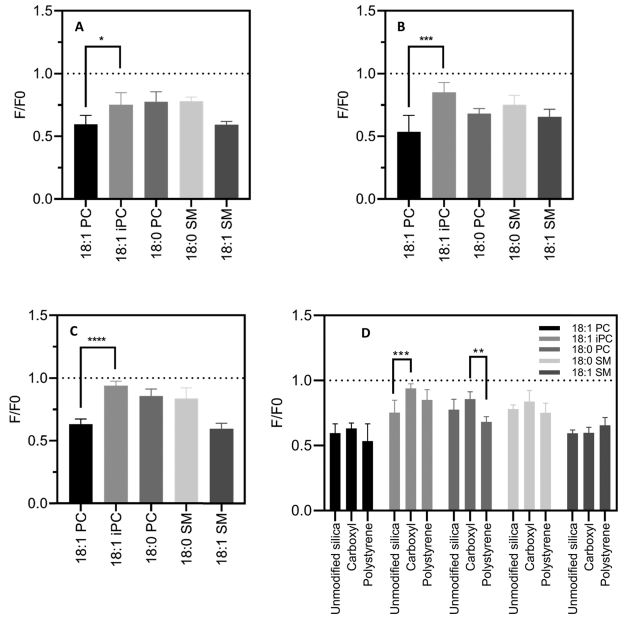

Figure 3. Particle association with single-component vesicles at a concentration of 134 pM (0.01 mg/mL) for silica nanoparticles and 246 pM (0.01 mg/mL) for polystyrene nanoparticles after 1 h of incubation examined by FRET for (A) unmodified silica, (B) unmodified polystyrene, and (C) carboxyl-modified silica. The fluorescein on particle surfaces was quenched by Rhod-DOPE (1 mol %) in vesicles upon colocalization. The ratio of fluorescein on nanoparticles in the absence of Rhod-DOPE fluorescence (F_0) to its fluorescence in the presence of Rhod-DOPE (F) was used as a measure of the nanoparticle association with vesicles. Error bars demonstrate the standard deviation from at least three independent experiments. (A) One-way ANOVA with Tukey's post hoc test was used for the pairwise comparison of F/F_0 values between different samples *P(18:1 PC vs 18:1 iPC) <0.01; (B) ***P(18:1 PC vs 18:1 iPC) <0.0001; (C) one-way ANOVA with Tukey's post hoc test was used for the pairwise comparison of F/F_0 values between different samples ****P(18:1 PC vs 18:1 iPC) <0.0001; and (D) two-way ANOVA with Tukey's post hoc was used for the multiple comparison of F/F_0 values between different samples, ***P(unmodified vs carboxyl) <0.0006 in 18:1 iPC vesicles, **P(carboxyl vs polystyrene) <0.003 in 18:0 PC vesicles. Note that the maximum achievable value for F/F_0 is 1.0 (dotted line).

each vesicle, but there were differences in nanoparticle binding to 18:1 iPC and 18:0 PC vesicles (Figure 3D).

Nanoparticles Induced Local Gelation in Vesicles That Are in Fluid Phase. To examine the effects of nanoparticles on the lipid packing of vesicles, DPH fluorescence anisotropy was used. A high value of anisotropy indicates a tight lipid packing of vesicles in the L_o phase, while a low anisotropy value denotes a loose lipid packing of vesicles in the L_d phase. First, the DPH anisotropy of vesicles in the absence of nanoparticles was measured. As expected, vesicles composed of 18:1 PC, 18:1 iPC, and 18:1 SM, which have cis unsaturation in their tails, showed a low DPH anisotropy with values ranging between 0.12 and 0.16, indicating a loose lipid packing. In contrast, 18:0 PC and 18:0 SM vesicles showed high anisotropy, demonstrating tight lipid packing (Figure 4A–C, black lines).

Vesicle anisotropy measured in the presence of particles revealed that nanoparticles are capable of altering lipid packing in vesicles, with the effect being highly dependent on the nanoparticle surface properties and vesicle structure. No

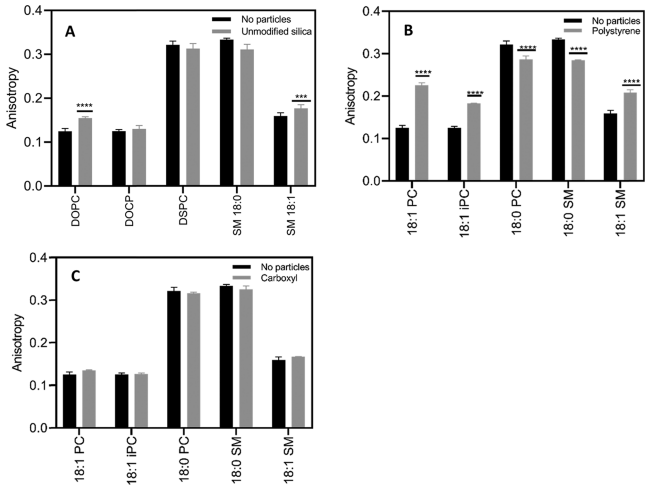

Figure 4. Effects of nanoparticles on the lipid packing of single-component vesicles measured using DPH anisotropy at a nanoparticle concentration of 1340 pM (0.1 mg/mL) for silica and 2460 pM (0.1 mg/mL) for polystyrene after 1 h of incubation: (A) unmodified silica particles, (B) unmodified polystyrene particles, and (C) carboxyl-modified silica particles. All experiments were performed with a lipid concentration of 500 μM using 0.2 mol % DPH to measure anisotropy. Error bars demonstrate the standard deviation from at least three independent experiments. Two-way ANOVA with Dunnett's post hoc test was used for comparing DPH anisotropy values with control (i.e., no particles): (A) ****P(18:1 PC) <0.0001 and **P(18:1 SM) <0.005; (B) ****P(18:1 PC) <0.0001, ****P(18:1 iPC) <0.0001, ****P(18:0 PC) <0.0001, ****P(18:0 SM) <0.0001, and ****P(18:1 SM) <0.0001; and (C) no significant difference was observed ($p > 0.05$).

appreciable change in DPH anisotropy was observed after vesicle exposure to nanoparticles at a particle concentration of 0.01 mg/mL (134 pM for silica and 246 pM for polystyrene) (Figure S5), which is the same concentration used for the leakage and FRET experiments. However, increasing the concentration of particles to 0.1 mg/mL (1340 pM for silica and 2460 pM for polystyrene) induced significant changes in vesicle anisotropy. This observation indicates that the number of nanoparticles at low concentration was not sufficient to induce measurable changes in lipid packing in vesicles. This is because the anisotropy value was measured and averaged over the entire vesicle surface for all particles and the intact regions on the vesicle surface could have negated nanoparticle-induced changes in anisotropy. Unmodified silica particles significantly increased the anisotropy of 18:1 PC and 18:1 SM vesicles, suggesting that exposure to these nanoparticles increases the packing of lipids in these vesicles (Figure 4A). Polystyrene nanoparticles had a similar effect on all vesicles containing unsaturated lipids, 18:1 PC, 18:1 iPC, and 18:1 SM vesicles, resulting in higher anisotropy (Figure 4B). It should be noted that although no appreciable increase was observed in the anisotropy of iPC vesicles by unmodified silica, polystyrene increased the anisotropy of iPC vesicles significantly. Polystyrene also reduced the anisotropy of vesicles containing saturated lipids, 18:0 PC and 18:0 SM vesicles (Figure 4B). In contrast, carboxyl-modified silica nanoparticles did not alter the anisotropy of any of the vesicles, even 18:1 SM vesicles, which these particles significantly disrupted (Figure 4C). While reconstruction of PC vesicles by negatively charged nanoparticles has been previously reported,[38] these findings indicate that nanoparticle effects on vesicle reconstruction are highly

https://dx.doi.org/10.1021/acs.langmuir.0c00295
Langmuir 2020, 36, 4923−4932

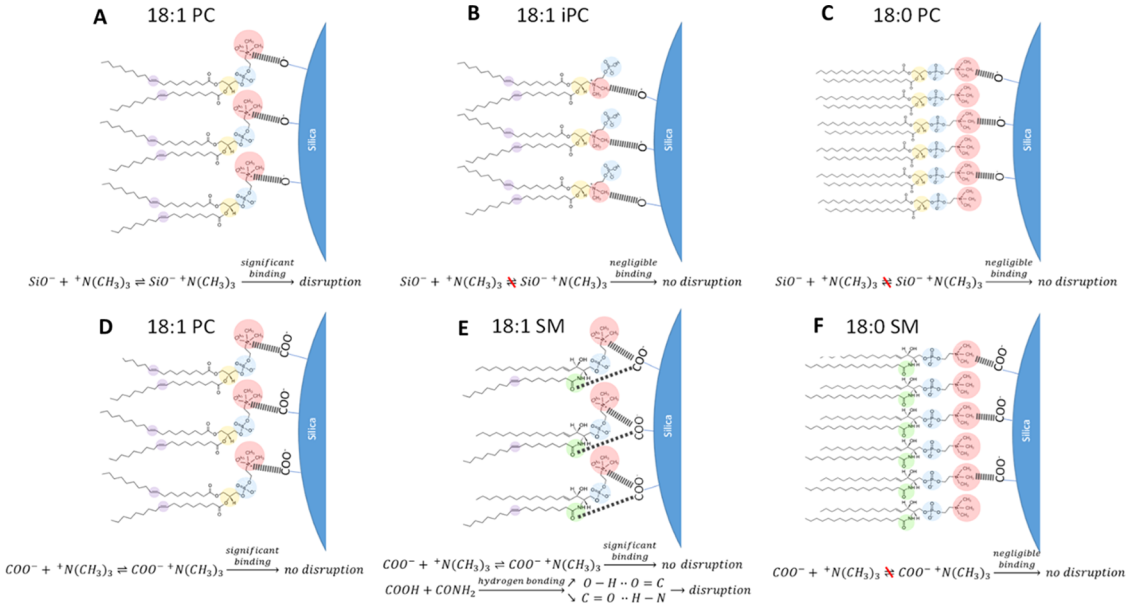

Figure 5. Summary of the proposed mechanisms through which silica nanoparticles bind to and disrupt single-component vesicles. (A) Interaction of unmodified silica nanoparticles with 18:1 PC: significant binding occurs between silanol on silica and choline chemical moieties, leading to vesicle disruption. (B) Interaction of unmodified silica nanoparticles with 18:1 iPC: binding of silanol to choline is reduced as choline is not accessible at the extremity of 18:1 iPC, resulting in a reduction in vesicle disruption. (C) Interaction of unmodified silica nanoparticles with 18:0 PC: the high tilt angle of phosphocholine, as well as the tight lipid packing of 18:0 PC, does not allow for silanol to reach the binding site in choline, leading to a low nanoparticle binding and vesicle disruption. (D) Interaction of carboxyl-modified silica nanoparticles with 18:1 PC: significant binding occurs between choline and carboxyl chemical moieties, but does not lead to vesicle disruption. (E) Interaction of carboxyl-modified silica nanoparticles with 18:1 SM: significant hydrogen bonding occurs between carboxyl and amide preferentially, leading to vesicle disruption. (F) Interaction of carboxyl-modified silica nanoparticles with 18:0 SM: the high tilt angle of phosphocholine, as well as the tight lipid packing of 18:0 SM, does not allow carboxyl to reach the binding site, amide, leading to a low nanoparticle binding and vesicle disruption. Highlighted circles denote the chemical moieties on the lipid structure: red, blue, yellow, purple, and green denote trimethylammonium, phosphate, glycerol, cis unsaturation on carbon 9, and amide chemical groups, respectively.

dependent on both the nanoparticle surface chemical properties and the lipid chemical structure, similar to what was observed in the vesicle integrity and binding experiments.

Several studies have suggested that pure electrostatic forces between membranes and nanoparticles regulate nanoparticle−membrane interactions.[14,17,39] In the current study, through leakage, binding, and anisotropy experiments, we show that, while electrostatic forces are important, the nature of the chemical moieties on the nanoparticle surface and in the lipid structure plays an important role in nanoparticle binding to and disruption of the vesicles. In unmodified silica particles, ion pairing between silanol (SiO^-) in silica and trimethylammonium ($N(CH3)_3^+$) in the choline headgroup of PC vesicles leads to a strong interaction,[40,41] resulting in significant binding and disruption of the vesicles (Figures 2A and 3A). Results suggest a similar mechanism for polystyrene particles, in which the sulfonic group (SO_3^-) can strongly interact with the choline headgroup in PC vesicles, resulting in disruption (Figures 2B and 3B). Results with 18:1 iPC vesicles, in which the presence of phosphate (PO_4^{3-}) at the vesicle surface reduces nanoparticle binding and disruption, further corroborate these mechanisms (Figures 2 and 3). Similarly charged, carboxyl-modified silica nanoparticles did not disrupt 18:1 PC vesicles despite significant binding (Figures 2C and 3C). This observation suggests that carboxyl has a weaker interaction with choline compared to silanol, which causes binding, but not disruption.

An important finding in this study is the role of the backbone in SM vs PC in governing nanoparticle−membrane interactions. The presence of the amide group in the sphingosine backbone and the choline in the lipid headgroup creates two possible binding sites in SM lipids for carboxyl-modified silica particles. While binding of carboxyl-modified silica particles to 18:1 SM and PC is similar (Figure 3C), the extent of dye leakage from 18:1 SM vesicles is significantly greater (Figure 2C). We attribute this particular interaction between carboxyl-modified silica and 18:1 SM vesicles to the strong hydrogen bonding between carboxyl and amide chemical moieties, converting the trans amide to the less stable cis amide, resulting in significant vesicle disruption.[42] Carboxyl-modified silica particles do not interact with 18:0 SM similarly to 18:1 SM vesicles, suggesting that particles do not "see" the amide group in the sphingosine backbone of 18:0 SM due to the tight lipid packing of these vesicles, as evidenced by anisotropy (Figure 4C). Therefore, it is not only the lipid headgroup but also the lipid backbone that modulates nanoparticle−membrane interactions.

Lipid packing is another important factor in nanoparticle-induced damage in single-component vesicles. Vesicles in a highly ordered state form a packed lipid structure, which is more resistant to disruption by nanomaterials. This packing also affects the ability of nanoparticles to bind to certain chemical moieties in lipids. The tilt angle of the phosphocholine headgroup in the gel phase is approximately in the range of 30−65°, while the tilt angle of phosphocholine in the fluid phase is approximately 0−3°.[38,43] The high tilt angle of phosphocholine and the tightly packed structure of vesicles composed of saturated lipids impede nanoparticle interaction with choline in the lipid headgroup, thereby decreasing nanoparticle binding to the vesicles. While the high level of

https://dx.doi.org/10.1021/acs.langmuir.0c00295
Langmuir 2020, 36, 4923−4932

packing in the 18:0 PC and SM vesicles is not representative of what is observed in the plasma membrane, it does provide mechanistic information on the role of lipid packing in nanoparticle-induced membrane damage. Nanoparticle effects on highly ordered vesicles are in stark contrast with what is observed for vesicles in the L_d phase, as evidenced by significant differences in the binding of silica particles to 18:0 vs 18:1 SM and PC (Figure 3A,C). Nanoparticles associate with vesicles in the L_d phase in substantial amounts, leading to significant leakage due to a strong ion pairing facilitated by the low tilt angle of phosphocholine. In the process, nanoparticles also enhance the packing of lipids resulting in less fluid membranes, as evidenced by changes in the anisotropy of unsaturated vesicles after nanoparticle binding (Figure 4). An illustration of the proposed mechanisms by which nanoparticles bind to and disrupt vesicles is depicted in Figure 5. The reader is cautioned that, while the molecular interactions shown in this schematic are supported by the literature and the observations in the current study, they should still be considered as proposed mechanisms, until the molecular-level details are independently confirmed.

In the current study, the loss of vesicle integrity after exposure to nanomaterials is characterized by the leakage of dyes from the lumen of the vesicles. We attribute the mechanism for the dye leakage to nanoparticle-induced pore formation in the structure of the vesicles. We have previously shown, using a FRET-based assay, that silica nanoparticles induce pores in vesicles mimicking the outer leaflet of the plasma membrane of human erythrocytes.[23] This is in line with what is observed in the current study, with nanoparticles enhancing the anisotropy of vesicles in the L_o phase, causing gelation in vesicles at sites of nanoparticle binding, in which they caused leakage (Figure 4A,B). Increased lipid packing is associated with changes in the tilt angle of lipid headgroups, recruiting lipid tails to reduce the area per lipid, causing vesicle shrinkage and creation of pores. The gelation effect induced by carboxyl-modified silica nanoparticles in vesicles composed of unsaturated PCs was weak (Figure 4C), resulting in a lower leakage due to weak phase transition in vesicles. The conformational change in the amide group that is induced by carboxyl-modified particles is due to the formation of hydrogen bond, explaining the disruption of 18:1 SM by carboxyl-modified silica. This particular interaction differs from ion pairing between choline and silanol, as evidenced by only a slight increase in the fluorescence anisotropy of 18:1 SM, despite significant leakage. It is likely that the amide conformational change results in the formation of supported lipid bilayer (SLB) on nanoparticle surfaces, as has been reported in several studies.[44−46]

CONCLUSIONS

The interest in understanding the mechanisms of nanoparticle-induced cell toxicity has led to increasing efforts to elucidate how nanomaterials disrupt the integrity of the cell plasma membrane. In the current study, single-component vesicles were used to examine how phospholipid composition regulates nanoparticle−vesicle interactions. This study elucidates that nanoparticle-induced membrane damage is regulated by specific intermolecular interactions, namely, ion pairing and hydrogen bonding, between nanoparticles and vesicles. These interactions depend on specific nanoparticle surface moieties, even for nanoparticles of the same charge, and are highly affected by the lipid chemical structure. Strong ion pairing between silanol, or sulfonic, and trimethylammonium drives the disruption of PC vesicles by nanoparticles. This interaction is weaker in carboxyl-modified particles, resulting in binding, but no disruption. Carboxyl-modified particles form hydrogen bonds with amide in the sphingosine backbone, leading to its disruption, but do not disrupt the glycerol backbone. Acyl chain saturation abrogates the disruptive effects of nanoparticles through impeding molecular interactions, by increasing the phosphocholine tilt angle and vesicle lipid packing. In summary, vesicle structure and nanoparticle surface chemistry are both important in regulating nanoparticle-induced membrane damage. These findings are important in explaining the mechanisms of toxicity of nanomaterials to biological membranes.

ASSOCIATED CONTENT

Supporting Information

The Supporting Information is available free of charge at https://pubs.acs.org/doi/10.1021/acs.langmuir.0c00295.

Additional nanoparticle characterization, vesicle leakage results at different nanoparticle concentrations, raw data for FRET experiments, and fluorescence anisotropy at low nanoparticle concentrations (PDF)

(PDF)

AUTHOR INFORMATION

Corresponding Author

Amir M. Farnoud − *Department of Chemical and Biomolecular Engineering and Biomedical Engineering Program, Ohio University, Athens, Ohio 45701, United States;* orcid.org/0000-0001-8572-6588; Phone: (740) 593-1426; Email: farnoud@ohio.edu; Fax: Fax

Authors

Saeed Nazemidashtarjandi − *Department of Chemical and Biomolecular Engineering, Ohio University, Athens, Ohio 45701, United States*

Amid Vahedi − *Department of Chemical and Biomolecular Engineering, Ohio University, Athens, Ohio 45701, United States*

Complete contact information is available at: https://pubs.acs.org/10.1021/acs.langmuir.0c00295

Notes

The authors declare no competing financial interest.

ACKNOWLEDGMENTS

This work was supported by the NIH grant R15ES030140 and the NSF grant CBET1903568. Financial support from the Russ College of Engineering and Technology and the Department of Chemical and Biomolecular Engineering at Ohio University is also acknowledged.

REFERENCES

(1) Napierska, D.; Thomassen, L. C. J.; Lison, D.; Martens, J. A.; Hoet, P. H. The Nanosilica Hazard: Another Variable Entity. *Part. Fibre Toxicol.* **2010**, *7*, 39.

(2) Baalousha, M.; Yang, Y.; Vance, M. E.; Colman, B. P.; McNeal, S.; Xu, J.; Blaszczak, J.; Steele, M.; Bernhardt, E.; Hochella, M. F. Outdoor Urban Nanomaterials: The Emergence of a New, Integrated, and Critical Field of Study. *Sci. Total Environ.* **2016**, *557*−*558*, 740−753.

(3) Yan, Y.; Such, G. K.; Johnston, A. P. R.; Best, J. P.; Caruso, F. Engineering Particles for Therapeutic Delivery: Prospects and Challenges. *ACS Nano* **2012**, *6*, 3663−3669.
(4) Doane, T. L.; Burda, C. The Unique Role of Nanoparticles in Nanomedicine: Imaging, Drug Delivery and Therapy. *Chem. Soc. Rev.* **2012**, *41*, 2885−2911.
(5) Doğangün, M.; Hang, M. N.; Troiano, J. M.; McGeachy, A. C.; Melby, E. S.; Pedersen, J. A.; Hamers, R. J.; Geiger, F. M. Alteration of Membrane Compositional Asymmetry by LiCoO2 Nanosheets. *ACS Nano* **2015**, *9*, 8755−8765.
(6) Tong, X.; Moradipour, M.; Novak, B.; Kamali, P.; Asare, S. O.; Knutson, B. L.; Rankin, S. E.; Lynn, B. C.; Moldovan, D. Experimental and Molecular Dynamics Simulation Study of the Effects of Lignin Dimers on the Gel-to-Fluid Phase Transition in DPPC Bilayers. *J. Phys. Chem. B* **2019**, *123*, 8247−8260.
(7) Warren, E. A. K.; Payne, C. K. Cellular Binding of Nanoparticles Disrupts the Membrane Potential. *RSC Adv.* **2015**, *5*, 13660−13666.
(8) Arvizo, R. R.; Miranda, O. R.; Thompson, M. A.; Pabelick, C. M.; Bhattacharya, R.; Robertson, J. D.; Rotello, V. M.; Prakash, Y. S.; Mukherjee, P. Effect of Nanoparticle Surface Charge at the Plasma Membrane and Beyond. *Nano Lett.* **2010**, *10*, 2543−2548.
(9) Leroueil, P. R.; Hong, S.; Mecke, A.; Baker, J. R.; Orr, B. G.; Banaszak Holl, M. M. Nanoparticle Interaction with Biological Membranes: Does Nanotechnology Present a Janus Face? *Acc. Chem. Res.* **2007**, *40*, 335−342.
(10) Hong, S.; Leroueil, P. R.; Janus, E. K.; Peters, J. L.; Kober, M.-M.; Islam, M. T.; Orr, B. G.; Baker, J. R.; Banaszak Holl, M. M. Interaction of Polycationic Polymers with Supported Lipid Bilayers and Cells: Nanoscale Hole Formation and Enhanced Membrane Permeability. *Bioconjugate Chem.* **2006**, *17*, 728−734.
(11) Zhao, Y.; Sun, X.; Zhang, G.; Trewyn, B. G.; Slowing, I. I.; Lin, V. S.-Y. Interaction of Mesoporous Silica Nanoparticles with Human Red Blood Cell Membranes: Size and Surface Effects. *ACS Nano* **2011**, *5*, 1366−1375.
(12) Farnoud, A. M.; Nazemidashtarjandi, S. Emerging Investigator Series: Interactions of Engineered Nanomaterials with the Cell Plasma Membrane; What Have We Learned from Membrane Models? *Environ. Sci.: Nano* **2019**, *6*, 13−40.
(13) Chen, Y.; Bothun, G. D. Cationic Gel-Phase Liposomes with "Decorated" Anionic SPIO Nanoparticles: Morphology, Colloidal, and Bilayer Properties. *Langmuir* **2011**, *27*, 8645−8652.
(14) Alkhammash, H. I.; Li, N.; Berthier, R.; de Planque, M. R. R. Native Silica Nanoparticles Are Powerful Membrane Disruptors. *Phys. Chem. Chem. Phys.* **2015**, *17*, 15547−15560.
(15) Liu, X.; Chen, K. L. Interactions of Graphene Oxide with Model Cell Membranes: Probing Nanoparticle Attachment and Lipid Bilayer Disruption. *Langmuir* **2015**, *31*, 12076−12086.
(16) Laurencin, M.; Georgelin, T.; Malezieux, B.; Siaugue, J.-M.; Ménager, C. Interactions Between Giant Unilamellar Vesicles and Charged Core−Shell Magnetic Nanoparticles. *Langmuir* **2010**, *26*, 16025−16030.
(17) Mornet, S.; Lambert, O.; Duguet, E.; Brisson, A. The Formation of Supported Lipid Bilayers on Silica Nanoparticles Revealed by Cryoelectron Microscopy. *Nano Lett.* **2005**, *5*, 281−285.
(18) Yang, K.; Ma, Y.-Q. Computer Simulation of the Translocation of Nanoparticles with Different Shapes across a Lipid Bilayer. *Nat. Nanotechnol.* **2010**, *5*, 579−583.
(19) Moghadam, B. Y.; Hou, W.-C.; Corredor, C.; Westerhoff, P.; Posner, J. D. The Role of Nanoparticle Surface Functionality in the Disruption of Model Cell Membranes. *Langmuir* **2012**, *28*, 16318−16326.
(20) Adib, A. A.; Nazemidashtarjandi, S.; Kelly, A.; Kruse, A.; Cimatu, K.; David, A. E.; Farnoud, A. M. Engineered Silica Nanoparticles Interact Differently with Lipid Monolayers Compared to Lipid Bilayers. *Environ. Sci.: Nano* **2018**, *5*, 289−303.
(21) Leidl, K.; Liebisch, G.; Richter, D.; Schmitz, G. Mass Spectrometric Analysis of Lipid Species of Human Circulating Blood Cells. *Biochim. Biophys. Acta, Mol. Cell Biol. Lipids* **2008**, *1781*, 655−664.
(22) Zehethofer, N.; Bermbach, S.; Hagner, S.; Garn, H.; Müller, J.; Goldmann, T.; Lindner, B.; Schwudke, D.; König, P. Lipid Analysis of Airway Epithelial Cells for Studying Respiratory Diseases. *Chromatographia* **2015**, *78*, 403−413.
(23) Nazemidashtarjandi, S.; Farnoud, A. M. Membrane Outer Leaflet Is the Primary Regulator of Membrane Damage Induced by Silica Nanoparticles in Vesicles and Erythrocytes. *Environ. Sci.: Nano* **2019**, *6*, 1219−1232.
(24) Bretscher, M. S. Asymmetrical Lipid Bilayer Structure for Biological Membranes. *Nat. New Biol.* **1972**, *236*, 11−12.
(25) Devaux, P. F.; Morris, R. Transmembrane Asymmetry and Lateral Domains in Biological Membranes. *Traffic* **2004**, *5*, 241−246.
(26) Bigdelou, P.; Farnoud, A. M. Induction of Eryptosis in Red Blood Cells Using a Calcium Ionophore. *J. Visualized Exp.* **2020**, No. e60659.
(27) Schmid, K.; Riediker, M. Use of Nanoparticles in Swiss Industry: A Targeted Survey. *Environ. Sci. Technol.* **2008**, *42*, 2253−2260.
(28) Rosen, J.; Landriscina, A.; Friedman, A. J. Nanotechnology-Based Cosmetics for Hair Care. *Cosmetics* **2015**, *2*, 211−224.
(29) Sampaio, S.; Maia, F.; Gomes, J. R. Diffusion of Coloured Silica Nanoparticles into Human Hair. *Coloration Technology* **2011**, *127*, 55−61.
(30) Clark, H. A. Paint Compositions. U.S. Patent US39764971976.
(31) Shamei, A.; Parvinzadeh, M.; Alimohammadi, F. Water-Resistant Silica-Embedded Textiles. U.S. Patent US20110287245A12011.
(32) Florence, A. T.; Hillery, A. M.; Hussain, N.; Jani, P. U. Factors Affecting the Oral Uptake and Translocation of Polystyrene Nanoparticles: Histological and Analytical Evidence. *J. Drug Targeting* **1995**, *3*, 65−70.
(33) Kulkarni, S. A.; Feng, S.-S. Effects of Particle Size and Surface Modification on Cellular Uptake and Biodistribution of Polymeric Nanoparticles for Drug Delivery. *Pharm. Res.* **2013**, *30*, 2512−2522.
(34) Zhenxing, H.; Xiaowei, Y.; Junliang, L.; Yuping, Y.; Ling, W.; Yanwei, Z. An Investigation of the Effect of Sodium Dodecyl Sulfate on Quasi-Emulsifier-Free Emulsion Polymerization for Highly Monodisperse Polystyrene Nanospheres. *Eur. Polym. J.* **2011**, *47*, 24−30.
(35) Bakht, O.; Pathak, P.; London, E. Effect of the Structure of Lipids Favoring Disordered Domain Formation on the Stability of Cholesterol-Containing Ordered Domains (Lipid Rafts): Identification of Multiple Raft-Stabilization Mechanisms. *Biophys. J.* **2007**, *93*, 4307−4318.
(36) Pathak, P.; London, E. Measurement of Lipid Nanodomain (Raft) Formation and Size in Sphingomyelin/POPC/Cholesterol Vesicles Shows TX-100 and Transmembrane Helices Increase Domain Size by Coalescing Preexisting Nanodomains but Do Not Induce Domain Formation. *Biophys. J.* **2011**, *101*, 2417−2425.
(37) Lesniak, A.; Salvati, A.; Santos-Martinez, M. J.; Radomski, M. W.; Dawson, K. A.; Åberg, C. Nanoparticle Adhesion to the Cell Membrane and Its Effect on Nanoparticle Uptake Efficiency. *J. Am. Chem. Soc.* **2013**, *135*, 1438−1444.
(38) Wang, B.; Zhang, L.; Bae, S. C.; Granick, S. Nanoparticle-Induced Surface Reconstruction of Phospholipid Membranes. *Proc. Natl. Acad. Sci. U.S.A.* **2008**, *105*, 18171−18175.
(39) Dif, A.; Henry, E.; Artzner, F.; Baudy-Floc'h, M.; Schmutz, M.; Dahan, M.; Marchi-Artzner, V. Interaction between Water-Soluble Peptidic CdSe/ZnS Nanocrystals and Membranes: Formation of Hybrid Vesicles and Condensed Lamellar Phases. *J. Am. Chem. Soc.* **2008**, *130*, 8289−8296.
(40) Depasse, J.; Warlus, J. Relation between the Toxicity of Silica and Its Affinity for Tetraalkylammonium Groups. Comparison between Si02 and Ti02. *J. Colloid Interface Sci.* **1976**, *56*, 618−621.
(41) Kettiger, H.; Québatte, G.; Perrone, B.; Huwyler, J. Interactions between Silica Nanoparticles and Phospholipid Membranes. *Biochim. Biophys. Acta, Biomembr.* **2016**, *1858*, 2163−2170.
(42) Navarro, R. E.; Aguilera-Márquez, D.; Virués, C.; Inoue, M. Hydrogen Bonding between Carboxylic Acids and Amide-Based

https://dx.doi.org/10.1021/acs.langmuir.0c00295
Langmuir 2020, 36, 4923−4932

Macrocycles in Their Host−Guest Complexes. *Supramol. Chem.*. **2008**, *20*, 737−742.
(43) Somerharju, P.; Virtanen, J. A.; Cheng, K. H. Lateral Organisation of Membrane Lipids The Superlattice View. *Biochim. Biophys. Acta, Mol. Cell Biol. Lipids* **1999**, *1440*, 32−48.
(44) Ahmed, S.; Wunder, S. L. Effect of High Surface Curvature on the Main Phase Transition of Supported Phospholipid Bilayers on SiO2 Nanoparticles. *Langmuir* **2009**, *25*, 3682−3691.
(45) Savarala, S.; Ahmed, S.; Ilies, M. A.; Wunder, S. L. Stabilization of Soft Lipid Colloids: Competing Effects of Nanoparticle Decoration and Supported Lipid Bilayer Formation. *ACS Nano* **2011**, *5*, 2619−2628.
(46) Wang, H.; Drazenovic, J.; Luo, Z.; Zhang, J.; Zhou, H.; Wunder, S. L. Mechanism of Supported Bilayer Formation of Zwitterionic Lipids on SiO2 Nanoparticles and Structure of the Stable Colloids. *RSC Adv.* **2012**, *2*, 11336.

https://dx.doi.org/10.1021/acs.langmuir.0c00295
Langmuir 2020, 36, 4923−4932